DOI 10.5162/sensoren2019/5.4.4

Homodyne Vector Network Analysis as a Tool for the Real-Time Measurement of Electrical Material Parameter Distributions in the Field

Ronny Peter, Gerhard Fischerauer
Universität Bayreuth – Chair of Measurement and Control Systems
Universitätsstraße 30, 95447 Bayreuth, Germany

Abstract

The spatial distribution of electrical material parameters (e.g. permittivity and conductivity) can be a valuable indicator of the state of a chemical process or the condition of the processing system. Unfortunately, there are very few measurement systems that could handle this task in the field at low cost and with small shape factors. A potential solution currently under research for the determination of material parameter distributions is based on electromagnetic resonances inside chemical reactors. In the laboratory, vector network analyzers (VNA) and personal computers are used, which is expensive. This contribution reports on an application-specific stand-alone homodyne VNA with integrated data processing as an effort to transfer the laboratory-proven method to the field. The quality of the approach, validated by comparison with commercial VNAs, is shown to suffice for typical field applications.

Keywords: Material parameters, in-process measurement, vector network analyzer, field application.

Introduction

Synthetic fertilizers, processing of crude oil, pharmaceuticals, and exhaust gas treatment are just a few important application examples for the use of chemical reactions [1]. To run the processes with high efficiencies, one needs to know the process state. This includes the spatial distribution of the reactants and of thermodynamic variables such as temperature.

By way of an example, consider a three-way-catalytic (TWC) converter. It consists of a ceramic honeycomb carrier coated with a catalytically activated oxygen storage component, all placed in a metallic housing. When lean (oxygen-rich) exhaust gases flow through the TWC, its oxygen storage component stores the excess oxygen to prevent the generation of nitrogen oxides. In rich (oxygen-deficient) atmospheres, the storage component releases oxygen to burn excess hydrocarbon and carbon monoxide molecules. It is evident that the relative oxygen storage level (ROSL) in the TWC is an important process parameter. Knowing it allows one to better control the efficiency of the internal combustion engine (ICE) and its emissions by running it with alternately lean and rich air-fuel mixtures.

The state of the art is to indirectly monitor the integral ROSL by lambda probes mounted upstream and downstream of the TWC and measuring the air-fuel ratio in the exhaust gas [2]. A direct and spatially resolved ROSL measurement can be based on the Raman scattering of light, but such systems are expensive and limited to point measurements [3]. Another method is microwave imaging which reconstructs a 2- or 3-dimensional distribution of material parameters by evaluating the electric field inside a metallic enclosure [4]. However, it is hard to sample the electric field at sufficiently many points in a running process and the reconstruction requires substantial computational time.

Another microwave-based method is the use of resonances in a microwave cavity. A metallic enclosure (e.g., the housing of a TWC) serves as the resonant cavity [5] (Fig. 1). The frequencies at which resonances occur are influenced by the electrochemical material parameters inside the cavity. We have dealt with several aspects of this method [6], [7], but the availability of low-cost equipment suitable for field (in-process) use remains an open issue. Potentially viable approaches include the use of mobile-phone equipment [8] and of application-specific scalar network analysis [9].

In the following, we describe a third approach, viz., an application-specific VNA. This includes the background of the cavity perturbation method, our measurement system concept, its implementation, and validation results.

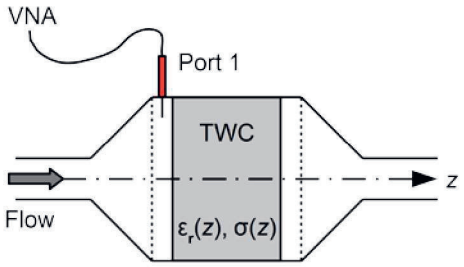

Fig. 1: Schematic drawing of a TWC used as resonant cavity.

The Cavity Resonator Method

Resonant cavities have been used for decades to determine material parameters. The cavity is either completely filled with a homogeneous sample (whole-medium perturbation, WMP) or loaded with a small sample (small-sample perturbation, SSP) [10]. The latter approach does not lend itself for in-process measurements as the sample needs to be prepared and precisely placed inside the cavity. The WMP method is better suited for in-process monitoring, but only so if the process provides homogeneous conditions. This is not always the case.

Axially varying material parameters inside a cavity may be resolved by evaluating several cavity resonances [6]. (Note that in many tubular reactors the material parameters are inhomogeneous in the direction of the flow but can be assumed to be homogeneous over the cross-section with little error [1], [2].) During the reconstruction of the material parameter distribution from the measured resonance parameters, the cavity is approximated by a discretized model with *N* homogeneous sections (Fig. 2). The reconstruction algorithm optimizes the material parameters such that the model predicts the cavity resonances with the least possible error in comparison with the measured data. This approximates the continuous material parameter variation in the axial direction by a stepwise constant distribution.

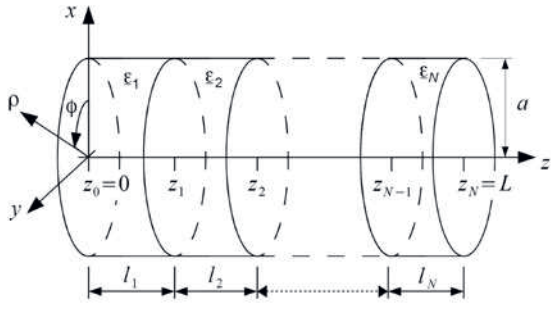

Fig. 2: Discretized cavity model used for the reconstruction of the material parameter distribution inside a cavity.

The method only requires the solution of an (over-)determined system of linear equations. The algorithm is simple and fast enough to be executed on a microcontroller in real-time.

When comparing simulated and measured cavity resonance properties, care has to be exercised that the simulated and measured objects are the same. The cavity is connected to a VNA by a coupling structure. The VNA outputs scattering (S-)parameter spectra, from which resonance curves are constructed. These curves lead to resonance parameters, such as resonance frequencies or Q-factors, by curve fitting [11]. As the coupling influences the resonance parameters – the cavity is said to be loaded –, this influence must be removed from the measured data by de-embedding before the results can be compared with the predictions of the simulation. The distinction between loaded and unloaded resonance parameters is especially important in field applications, which restrict one's control over sample sizes and coupling conditions.

Application-Specific Homodyne VNA

S-parameters can be scalar (magnitude only) or "vectorized", i.e., complex-valued (magnitude and phase). A good de-embedding of coupling effects is usually only achieved with methods based on complex S-parameters [7]. Commercial VNAs are too expensive and bulky for in-process applications in vehicles and similar environments. Measurement solutions for such applications have to meet the following requirements:

- measure complex S-parameters accurately enough for the extraction of resonance parameters
- operate in the low GHz range
- allow measuring times below 1 s
- be low-cost
- be low-profile
- have computational power commensurate with real-time material parameter extraction

Modern commercial VNAs use a (super-) heterodyne receiver design (Fig. 3) [12]. It mixes the RF signal produced by a voltage-controlled oscillator (VCO) and then reflected from the device under test (DUT; here: the cavity resonator) with a local-oscillator (LO) signal to obtain an intermediate frequency (IF). The latter is then sampled with a fast analog-to-digital-converter (ADC). The architecture is rather expensive because it requires two phase-synchronized RF sources, a fast ADC, and a field programmable gate array (FPGA) or a digital signal processor (DSP) to process

the large amounts of data produced by the ADC in real-time. This processing consists mainly of filtering and a fast Fourier-transformation (FFT).

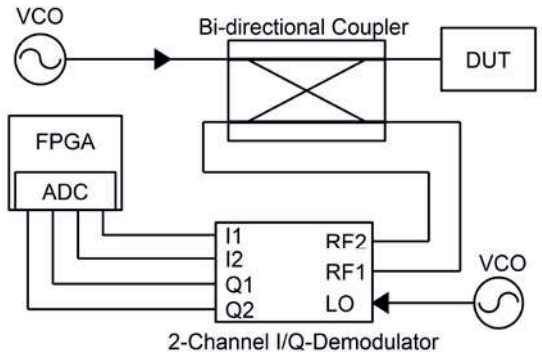

Fig. 3: Schematic drawing of a heterodyne VNA.

A less expensive architecture uses a homodyne receiver (Fig. 4). It mixes the reflected RF signal down to the baseband ($f_{IF} = f_{RF} - f_{LO} = 0$). Hence, a single oscillator can act as both RF and LO source, one can use a slower (less expensive) ADC, one needs no FFT, and a single measurement of the baseband signal suffices. A rather simple microcontroller (MCU) is suited for this task.

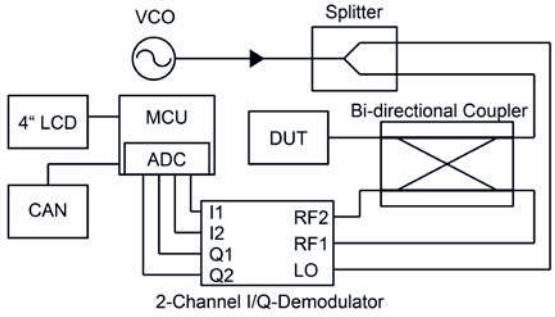

Fig. 4: Schematic drawing of a homodyne VNA.

The main disadvantage of the homodyne design is the LO leakage [13]. The self-mixing of the LO signal with the leaked LO signal produces a DC offset which will be superimposed on the DC signal resulting from the measurement. Another disadvantage is the higher pink noise level, compared to a heterodyne receiver. The resulting difficulty of a homodyne VNA to cope with very small signals is, however, inconsequential for resonance parameter measurements.

We have designed and implemented an application-specific homodyne VNA (Fig. 5). It comprises a digital programmable phase-locked loop (PLL) with a VCO as RF source, a 16-bit ADC with SPI-Interface for sampling, a bi-directional coupler, and an IQ-demodulator IC. The heart of the system is the STM32F7 development board running at 216 MHz. The parts list is completed by several amplifiers, filters, and power splitters. The only part costing more than 10 euros in large quantities is the MCU.

The system meets the following specifications:

- frequency range from 1 to 2.5 GHz (limited only by bi-directional coupler)
- measuring time ca. 311 ms for a 101-point spectrum
- resolution 10 kHz
- maximum of 10,001 frequency points
- built-in resonance parameter extraction

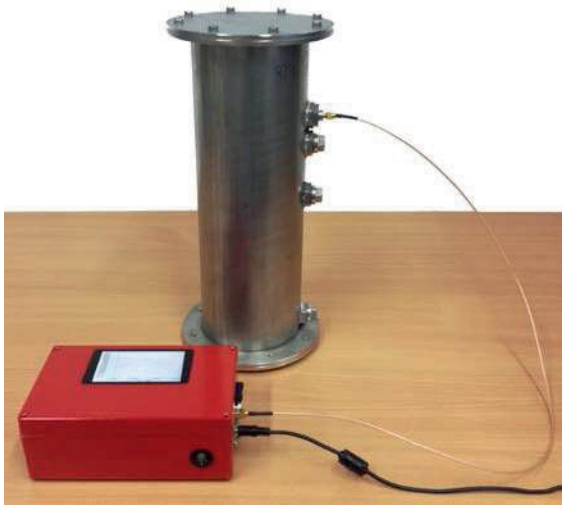

Fig. 5: Application-specific VNA coupled to a circular cylindrical cavity resonator.

Comparison with Commercial VNAs

The application-specific VNA (A) was validated by comparison with an Agilent N5230A PNA-L 300kHz-20GHz (B) and a Rohde&Schwarz ZVRe 9kHz-4GHz (C). Unless noted otherwise, the tests were performed with 6,001-point spectra from 1.4 to 2 GHz (frequency step size 100 kHz). All investigated cavities had at least three resonances in this frequency range. The VNAs were one-port calibrated with known calibration elements (short, open, match) [14, p. 484]. The calibration elements used for calibration of VNA A (Rohde&Schwarz ZV-Z132) were assumed to be ideal (except for offset). All measurements were taken with an averaging factor of 10.

Fig. 6 shows the measured negative return loss of various shorted attenuators. The error-less results would be flat lines at twice the nominal attenuation.

It is obvious that the application-specific VNA A performs the better, the higher the input signal level. Return-loss spectra at levels of about 20 dB show a somewhat higher ripple than spectra measured by the commercial VNA B,

and at 30 to 40 dB, the spectra are corrupted by considerable noise.

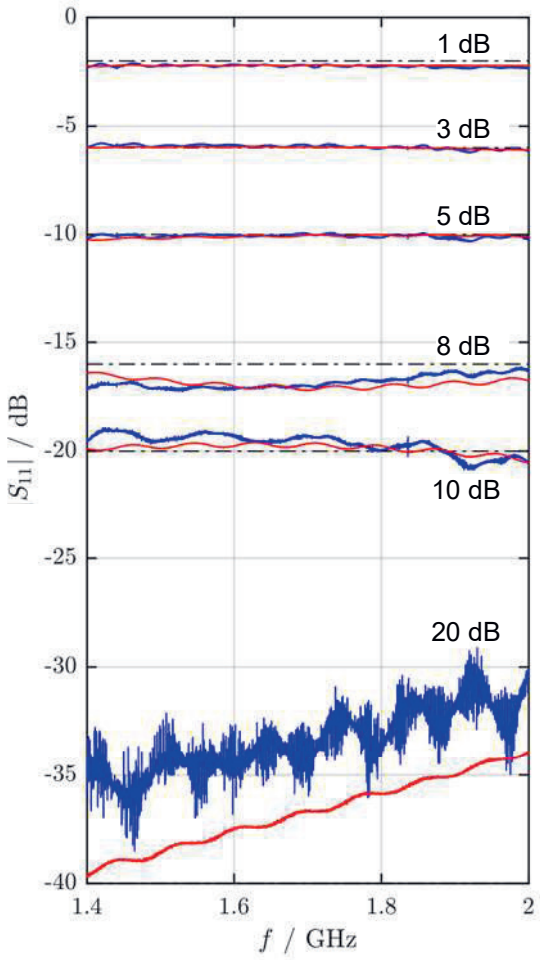

Fig. 6: Return-loss measurements on various shorted attenuators (attenuation as noted in the chart). Blue lines: VNA A. Red lines: VNA B.

What is also evident, however, is the fact that the application-specific VNA is very well suited for the extraction of resonance parameters from typical resonance peaks. Such typical peaks are associated with return losses below about 10 dB for most coupled cavities.

Fig. 6 is an indication of the magnitude error in the application-specific VNA A. To also quantify the phase error, we computed the error vector magnitude (EVM), i.e., the magnitude of the difference between the complex-valued phasors output by VNAs A and B. This was done for every attenuator measured for Fig. 6. The worst-case value at each frequency is shown in Fig. 7. The average worst-case EVM was -38.3 dB, which convincingly demonstrates the practical usability of VNA A.

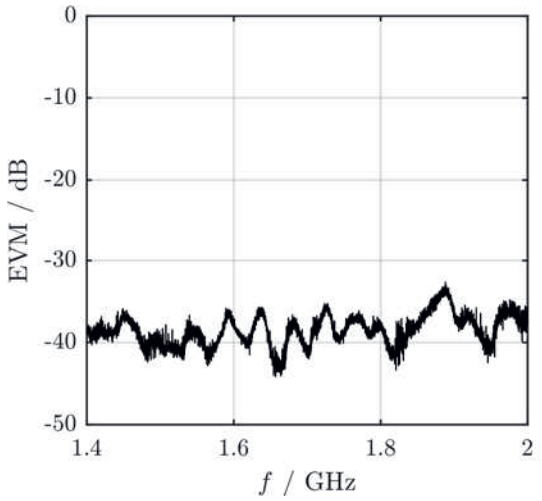

Fig. 7: Worst-case EVM of the VNA-A results for the shorted attenuators measured for Fig. 6.

Further tests were conducted with various cavity resonators as DUTs (Fig. 8). The cavities were of different shape (circular cylindrical and rectangular), of different length (365 mm to 412 mm), coupled with different coupling structures, and filled with different materials.
Fig. 9 shows the negative return-loss spectra from an air-filled cavity with circular cross-section (cavity 4). The three resonance curves produced by VNAs A, B, and C look very similar. From these curves, the resonance parameters were calculated as described in [7, eqn. 1]. This was done by post-processing on a PC for VNAs B and C, whereas VNA A computed the results directly via the implemented MCU routines.

Fig. 8: Cavities used for the characterization of VNA A.

By way of an example, the resonance frequencies and Q-factors of the fundamental mode (TE_{101}) as determined by the three VNAs are listed in Table 1. The good agreement of the results further confirm the practical usability of the application-specific VNA A.

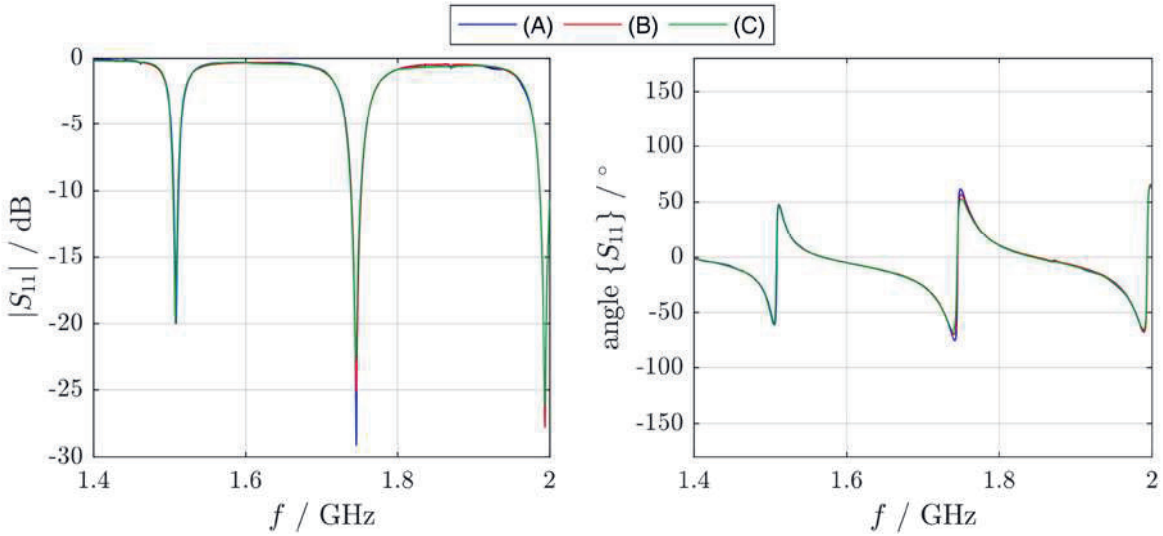

Fig. 9: Results of return-loss measurements with cavity no. 4.

Tab. 1: Resonance parameters of the fundamental mode (TE_{101}) in cavity 1 as determined with VNAs A to C.

VNA	f_{res} / GHz	Q_0
A	1.550874	1635.7
B	1.550687	1735.6
C	1.550785	1692.3

Similar comparisons were made for other modes (in the frequency range from 1.4 to 2 GHz) and other cavities. In the following, we restrict ourselves to the cavities 1 through 4 shown in Fig. 8. The average resonance parameters for each mode of each cavity were used as reference.

The fractional deviations of the resonance frequencies in cavity 1 from the average of the values returned by VNAs A, B, and C are presented in Fig. 10. It looks as if VNA A consistently returns resonance frequencies that are slightly too high, which may be a consequence of an offset error in its frequency base. As the fractional frequency deviation is only about 50 ppm (corresponding to 100 kHz for a 2-GHz resonance), the error may be neglected in practice, as reconstruction algorithms can cope with it [6]. Otherwise the error can be compensated in software by simply adding or subtracting an offset to or from the resonance frequency. Besides, the commercial VNAs B and C do not agree better with each other than with VNA A.

Whereas Fig. 10 is an indication of the accuracy of VNA A (measure of offset from the true value), Fig. 11 serves to judge its precision (measure of scattering around the mean result when an experiment is repeated). Fig. 11(a) shows the empirical standard deviation of the measured fractional resonance frequency deviations of all modes between 1.4 – 2 GHz in cavities 1 through 4, the reference being the average of the values returned by VNAs A, B, and C. Fig. 11(b) is an analogous representation of the standard deviation of the measured fractional Q-factor deviations for the same modes, the references being the average Q-factors returned by VNAs A, B, and C.

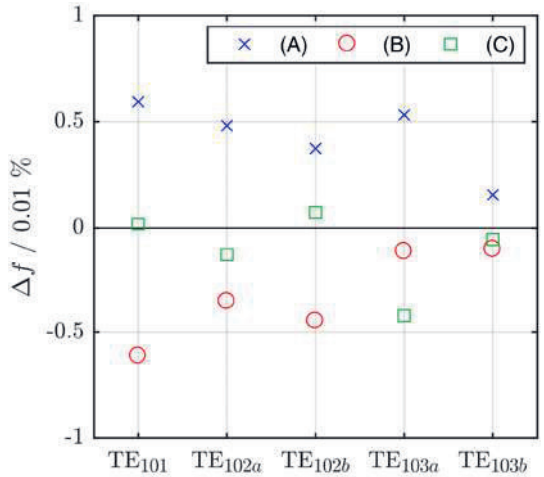

Fig. 10: Selected measured resonance frequencies in cavity 1, expressed as fractional deviation from the average of the values returned by VNAs A, B, and C. "a" and "b" denote split resonances associated with modes that are degenerate in the unloaded case.

Fig. 11 corroborates the notion that the application-specific VNA A allows one to determine resonance parameters with a performance comparable to that of commercial VNAs. This paves the way for in-situ field measurements at a price two orders of magnitude below the price of the laboratory equipment which has often been used to demonstrate the value of the cavity resonance method for material parameter measurements and process monitoring tasks.

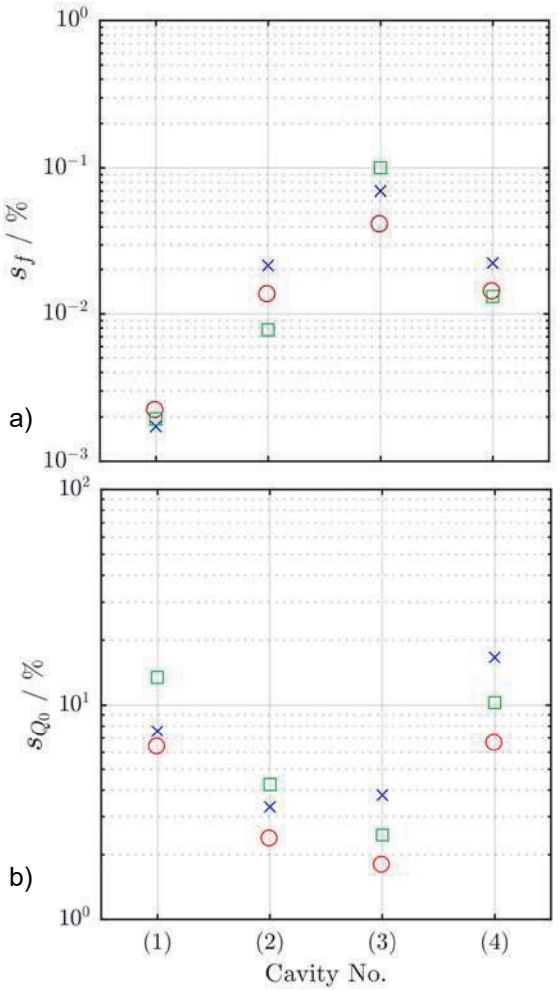

Fig. 11: Standard deviation of measured resonance parameters for all modes between 1.4 – 2 GHz in cavities 1 to 4. a) Fractional resonance frequency deviation. b) Fractional Q-factor deviation.

Measurement Time

The broadband measurements discussed above for validation purposes involve sweep times that may not be compatible with real-time applications. It is more likely that narrow bandwidths in the vicinity of known resonance frequencies would be used for process monitoring tasks to reduce the measurement time. Table 2 lists the required measurement time for ten repeated measurements with 101 discrete frequency points. Again, VNA A performs well in comparison with the commercial VNAs.

Tab. 2: Time required for ten measurements of a 101-point spectrum.

VNA	Measurement time / ms
A	311
B	25
C	520

The built-in parameter extraction algorithm of VNA A takes about 128 ms per resonance. This results in an overall time of 440 ms per resonance. An inhomogeneous cavity with four sections would require the characterization of four resonances, which would take 4×440 ms = 1.76 s. The time needed for the reconstruction of the material parameters of the four sections from the resonance parameters is difficult to state as the convergence of the iterative inversion algorithm depends on the estimated start values. In process monitoring applications, one may assume that the process state varies smoothly. In this case, the previous material parameter values may be taken as rather good start values for the subsequent estimation step. It is then safe to state that the overall time to measure the material parameter distribution in the four-section cavity would not exceed 5 s. This time scale suffices for all chemical processes the state changes of which are limited by mass flow, diffusion, temperature effects, and other slow phenomena.

An Application Example: Sand

As a practical application example, we demonstrate the characterization of sand. To this end, cavity 3 was uniformly filled with sand, and the resonance of the TE_{211} mode was evaluated. No attempt has been made to remove the coupling-stub influence by de-embedding.

Table 3 lists the real and imaginary parts of the relative permittivity estimated from the resonance parameters measured with VNA A, B, and C. The agreement is obvious.

To judge if the results are near the “true” parameter values, we compared the results to literature values. Unfortunately, the permittivity of sand depends on many parameters such as the composition of the sand, the grain size, the grain size distribution, wetness, etc. Table 3 cites two literature results which are respectively lower and higher than our permittivities. In any case, our measurements are in agreement with known literature data.

Tab. 3: Calculated permittivity of sand from extracted resonance parameters (cavity 3, TE_{211}).

VNA	ε'_r	ε''_r
A	2.7292	0.021
B	2.7353	0.018
C	2.7530	0.021
Ref. [15]	2.55	0.025
Ref. [16]	3.2	0.026

Conclusion

We have described the architecture and the performance of an application-specific low-cost homodyne VNA. It was demonstrated to be well suited for resonance-parameter determination and, by built-in software routines, for the reconstruction of material parameter distributions in cavities, which may serve to monitor the state of chemical processes.

The system was validated by comparison with commercial VNAs (which are more expensive by at least two orders of magnitude). Numerically, the resonance frequencies and Q-factors determined by the application-specific system typically deviated by less than 0.1 % and 10 % from the results of the commercial VNAs. Material parameters extracted from these resonance parameters agreed just as well.

The typical measurement time required for the reconstruction of a material parameter distribution in a process reactor used as cavity resonator is on the order of a few seconds.

Acknowledgment

Part of this work was funded by the Deutsche Forschungsgemeinschaft (DFG, German Research Foundation) – 389867475.

References

[1] A. Jess and P. Wasserscheid, *Chemical Technology*. Weinheim: Wiley-VCH, 2013.

[2] T.S. Auckenthaler, “Modelling and Control of Three-Way Catalytic Converters,” Ph.D. dissertation, ETH Zurich, Zurich, 2005.

[3] J. R. Ferraro, K. Nakamoto, and C. W. Brown, *Introductory Raman Spectroscopy.* 2nd Edition, Boston, MA, USA: Academic Press, 2003.

[4] M. Pastorino, *Microwave Imaging*. Hoboken, NJ, USA: Wiley, 2010.

[5] S. Schödel, R. Moos, M. Votsmeier, and G. Fischerauer, „SI-engine control with microwave-assisted direct observation of oxygen storage level in three-way catalysts“, *IEEE Trans. Control Syst. Technol.*, vol. 22, no. 6, pp. 2346–2353, Nov. 2014. DOI: 10.1109/TCST.2014.2305576.

[6] R. Peter and G. Fischerauer, “Measurement of Axially Inhomogeneous Permittivity Distributions in Resonant Microwave Cavities,” *IEEE Trans. Microw. Theory Techn.*, *in print*. DOI: 10.1109/TMTT.2019.2910177.

[7] R. Peter and G. Fischerauer, “De-Embedding Method for Strongly Coupled Cavities,” *IEEE Trans. Microw. Theory Techn.*, vol. 66, no. 4, pp. 2025–2033, Apr. 2018. DOI: 10.1109/TMTT.2018.2791934.

[8] L. F. Chen, C. K. Ong, C. P. Neo, V. V. Varadan, and V. K. Varadan, *Microwave Electronics: Measurement and Materials Characterization*. Chichester, U.K.: Wiley, 2004.

[9] I. Motroniuk, R. Królak, R. Stöber, and G. Fischerauer, “Wireless Communication-Based State Estimation of Automotive Aftertreatment Systems,” *Measurement*, vol. 106, pp. 245–250, Aug. 2017. DOI: 10.1016/j.measurement.2016.08.004.

[10] R. Królak and G. Fischerauer, “Scalar Reflectometry as a Means of Catalyst Monitoring Suitable for Field Applications,” *Measurement*, vol. 137, pp. 278–286, Apr. 2019. DOI: 10.1016/j.measurement.2019.01.030.

[11] D. Kajfez, “Q-Factor Measurement with Network Analyzer”, *IEEE Trans. Microw. Theory Techn.*, vol. 32, no. 7, pp. 666–670, Jul. 1984. DOI: 10.1109/TMTT.1984.1132751.

[12] N. B. Carvalho and D. Schreurs, *Microwave and Wireless Measurement Techniques*. New York, NY, USA: Cambridge Univ. Press, 2013.

[13] M. B. Steer, *Microwave and RF Design: A Systems Approach.* Herndon, VA: SciTech Publishing, 2010.

[14] S. A. Dyer (Ed.), *Survey of Instrumentation and Measurement*. New York, NY, USA: Wiley-Interscience, 2001.

[15] R. F. Harrington, *Time-Harmonic Electromagnetic Fields*. New York, NY, USA: IEEE Press, 2001.

[16] H. M. Al-Rizzo and H.T Al-Hafid, “Measurement of the Complex Dielectric Constant of Sand and Dust Particles at 11 GHz”, *IEEE Trans. Instrum. Meas.*, vol. 37, no. 1, pp. 110–113, Mar. 1988. DOI: 10.1109/19.2677.